https://doi.org/10.26599/FRICT.2026.9441342

Research Article

The influence of in situ modification strategies on the tribological behavior of polyurethane

Shimao Han[1,2], Peng Wei[2], Wei Xu[2], Luo Yue[2], Jie Cheng[1*], Fangxu Sun[3], Pengpeng Bai[2]

[1] School of Mechanical and Electrical Engineering, China University of Mining and Technology - Beijing, Beijing, China

[2] State Key Laboratory of Tribology in Advanced Equipment, Department of Mechanical Engineering, Tsinghua University, Beijing 100084, China

[3] Ational Key Laboratory of Electromagnetic Energy, Naval University of Engineering, Wuhan, 430033, China

✉ Corresponding author. E-mail: jiecheng@cumtb.edu.cn (J. Cheng)

Received: April 13, 2026; Revised: October 22, 2026; Accepted: November 18, 2026

© The Author(s) 2026.

Just Accepted

Abstract

Water-lubricated polymer bearings are increasingly used in marine propulsion, yet achieving low friction, vibration attenuation, and durable wear resistance in corrosive, particle-contaminated water remains challenging. Here, we systematically compare physical blending and chemical grafting as in situ modification routes for polyurethane (PU) nanocomposites, focusing on mechanical strength, damping behavior, and water-lubricated tribological performance. Composites were synthesized by in situ

polymerization with pristine multi-walled carbon nanotubes (MWCNTs) or hydroxyl-functionalized MWCNTs (OH-MWCNTs). Structural characterization shows that OH-MWCNTs covalently bond to PU chains, whereas pristine MWCNTs interact mainly through physical dispersion. Both approaches improve PU performance relative to neat PU, but with distinct trade-offs. Chemical grafting strengthens the interface, leading to higher yield/tensile strength and stiffness, and is more suitable for load-bearing conditions requiring stronger interfacial stability. In contrast, physical blending better preserves chain mobility and ductility, giving superior friction reduction and vibration damping. Under water lubrication, the optimized physically blended composite forms a continuous and smooth transfer film, which reduces direct contact, interfacial shear, and wear, thereby achieving the best overall anti-friction, damping, and wear-resistant performance within the investigated systems. Excessive filler loading deteriorates performance because of nanotube agglomeration and defect formation. These results clarify the mechanical–damping–tribological structure–property relationships of PU nanocomposites and provide guidance for selecting modification strategies for water-lubricated polymer bearings.

Keywords: Polymer modification; Chemical grafting; Physical blending; Water lubrication

1. Introduction

Polymer materials have become indispensable tribological materials in modern mechanical equipment due to their excellent anti-friction and wear resistance as well as superior self-lubricating properties. They are widely applied in various motion pairs[1-4], such as bearings, biomimetic cartilage[5-7], gears [8], and sealing components[9]. Particularly in aerospace, marine engineering[10], and other fields, polymer friction pairs can operate stably under non-lubricated or water-lubricated conditions[11], demonstrating unique application advantages[12-15]. Especially in water-lubricated bearings for ship propellers, friction pairs must endure long-term service under complex operating conditions including seawater corrosive media[16], sand particle erosion, humid environments, and variable load impacts, which impose more stringent requirements on material wear resistance, interface stability, and structural integrity. Therefore, the development of polymer-based tribological materials capable of maintaining high reliability under water-lubricated environments has become an important research direction for efficient and environmentally friendly propulsion systems.

However, with the rapid development of high-end equipment manufacturing, mechanical systems are evolving toward higher speeds and heavier loads, and service environments are becoming increasingly complex and harsh. Under extreme working conditions such as extreme temperatures(≤

Just Accepted

−100℃ or ≥ 150℃), radiation, and corrosion, as well as severe friction conditions including high-speed heavy loads and impact loads, as well as severe friction conditions including high-speed heavy loads and impact loads, traditional polymer materials typically exhibit insufficient strength and poor wear resistance[17-21]. Their tribological performance can no longer meet application requirements, seriously constraining the performance enhancement and reliability assurance of high-end equipment. To address this challenge, nano-modification technology provides an effective approach for improving the tribological properties of polymers. As a cost-effective method, nano-modification significantly enhances the mechanical and tribological properties of materials even at low loading levels by introducing nano-fillers into polymer matrices and utilizing their high specific surface area effects and interface effects[4, 22, 23]. According to the bonding mode between fillers and polymer matrices, nano-modification is primarily classified into two categories: physical blending, which introduces fillers into polymers through mechanical mixing, melt blending, and other methods, featuring simple processing but weak interfacial interactions[24-27]; and chemical grafting, which connects nano-fillers to polymer molecular chains through covalent bonds, achieving stronger interfacial bonding and superior dispersion effects [28-32].

Polyurethane (PU), as an important class of thermoplastic elastomers, exhibits excellent vibration damping and fatigue resistance due to its viscoelastic characteristics imparted by the microphase separation structure of soft and hard segments[33-36], making it an ideal matrix material for studying nano-modification[37, 38]. More importantly, the –NCO groups in the hard segments of polyurethane can chemically react with hydroxyl- or carboxyl-containing nanoparticles[39, 40], providing a theoretical basis for chemical grafting modification[41, 42]. Recent years have witnessed numerous advances in polyurethane nano-modification: for instance, Zhou et al. reduced the friction coefficient by 45.1% and decreased the wear rate by 206% under conditions of 66 N and 0.54 m/s by incorporating 0.5 wt% MXene into polyurethane through physical blending[43]; Talapatra et al. incorporated graphene (Gr) into thermoplastic polyurethane (TPU) via physical blending and, combined with molecular dynamics simulations, revealed that interlayer sliding and interfacial shearing are the dominant friction-reducing mechanisms[44]. Li et al. introduced aniline oligomer-functionalized graphene oxide into PU via chemical grafting, reducing the friction coefficient from 0.35 to 0.028 (a 92% decrease) and decreasing the wear rate by nearly 88%[39]; Song et al. utilized the reaction between –NCO groups of isophorone diisocyanate (IPDI) and hydroxyl and carboxyl groups on GO surfaces to prepare covalently grafted IPDI-GO and

Just Accepted

composite it with PU, achieving approximately 87% increase in tensile strength and 33% improvement in elongation at break, while significantly enhancing thermal stability and mechanical properties[41]. In summary, both physical blending and chemical grafting modification methods can improve polyurethane performance, but significant differences exist in interfacial bonding strength[45-47], load transfer efficiency[37, 48], and transfer film formation mechanisms[49, 50]. Existing research has predominantly focused on performance optimization of individual modification methods. However, systematic comparisons between physical blending and chemical grafting remain scarce, particularly under identical dispersion conditions and equivalent filler contents, with respect to mechanical properties, tribological behavior, and vibration damping characteristics[51-53]. Without such controlled comparisons, the differential effects of the two modification strategies cannot be fairly evaluated, and nano-modification research continues to rely largely on empirical trial-and-error for formulation design, resulting in low efficiency and limited rational guidance for material selection.

Based on this background, this study addresses the development of high-performance water-lubricated bearings for marine applications by selecting polyurethane, a material commonly used for polymer bearing bushings, as the base material, and employing MWCNT and OH-MWCNT as two types of nano-fillers for different modification approaches. While maintaining consistent dimensions and structure, the interaction with the polyurethane matrix is regulated through surface hydroxylation. Composites were prepared via in-situ polymerization, and a systematic comparison was conducted to evaluate the effects of physical blending and chemical grafting on the tribological properties of polyurethane. Multi-walled carbon nanotubes primarily bond with the matrix through physical interactions, whereas hydroxylated multi-walled carbon nanotubes can chemically react with polyurethane molecular chains to form stable covalent bonds, representing two typical modification methods. This study aims to reveal the action mechanisms of different modification methods, explore the formation and failure mechanisms of transfer films through analysis of the microstructure, interfacial characteristics, mechanical properties, and tribological behavior of the composites, thereby providing theoretical references for the rational selection of nano-modification methods and the development of high-performance polymer tribological materials.

2.Materials and methods

2.1. Materials

Poly (tetramethylene ether glycol) (PTMEG, Mn ≈ 2000 g/mol),Toluene diisocyanate (TDI, 98 %)

Just Accepted

and 4,4'-methylene-bis-(2-chloroaniline) (MOCA, 98 %) were purchased from Aladdin Biochemical Technology Co., Ltd. (Shanghai, China). The OH-MWCNTs (white powder, 95 %, the length of about 10–30 nm, the diameter of about 10 to 20 nm, Hydroxyl content 3.06wt%) and the MWCNTs (white powder, 95 %, the length of about 10–30 nm, the diameter of about 10 to 20 nm) were purchased from XFNANO Materials Tech Co., Ltd (Nanjing, China).

2.2. Sample preparation

All samples were synthesized via in-situ polymerization to obtain polyurethane/ multi-walled carbon nanotube (PU/MWCNTs) composites. A total of eleven samples were fabricated, including neat polyurethane (PU1); composites containing 0.125, 0.25, 0.5, 1, and 2 wt% pristine multi-walled carbon nanotubes (MWCNTs), designated PUC2–PUC6; and composites incorporating 0.125, 0.25, 0.5, 1, and 2 wt% hydroxyl-functionalized MWCNTs (OH-MWCNTs), labeled PUO2–PUO6.

The synthesis procedure was carried out as follows. Polytetramethylene ether glycol (PTMEG, 25 g, Mn = 2000 g/mol) was mixed with the required amount of MWCNTs in a three-necked flask and mechanically stirred at 125 ℃ for 12 h to remove moisture and ensure uniform dispersion. The temperature was then lowered to 65 ℃ before adding 4.48 g of toluene diisocyanate (TDI), and the reaction was allowed to proceed for 1 h. The resulting mixture was transferred to a vacuum oven to eliminate air bubbles, forming a prepolymer that was maintained at 100 ℃. In parallel, 3.51 g of MOCA was melted at 125 ℃ for 1 h. The molten chain extender was rapidly added to the prepolymer with vigorous stirring for 3 min while simultaneous degassing was applied. Finally, the reaction mixture was poured into preheated silicone molds and cured at 100 ℃ for 12 h. The molded samples were post-cured at room temperature for 24 h prior to characterization.

Just Accepted

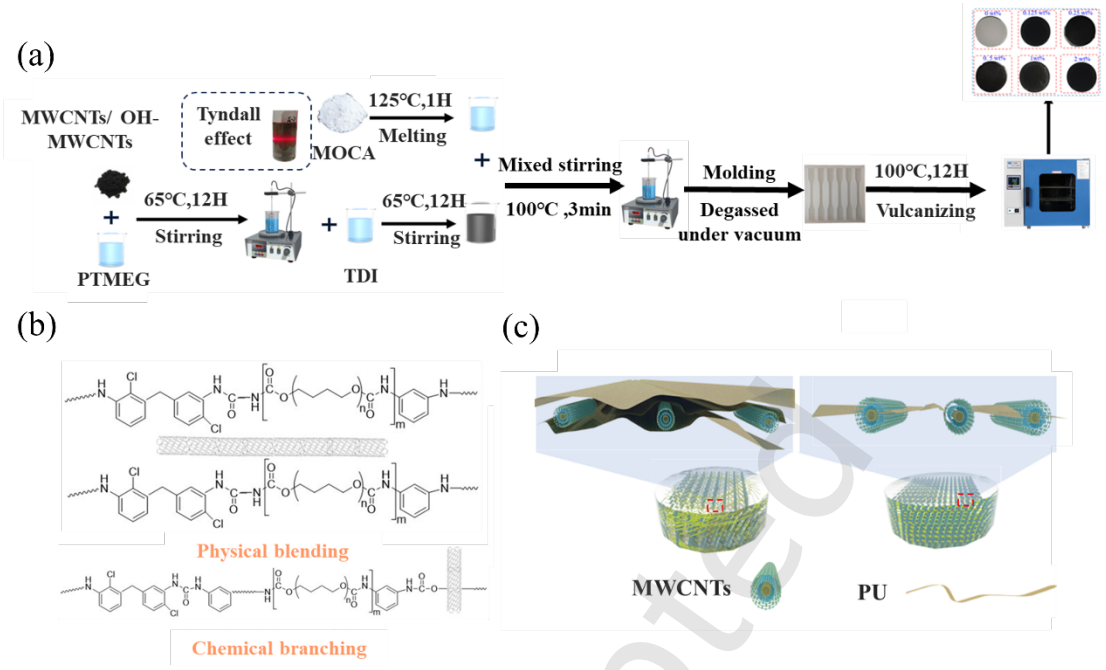


Figure 1. (a) Preparation process diagram of polyurethane composite materials; (b) molecular formula of polyurethane composite materials (c) schematic diagram of physical blending and chemical grafting in composite materials.

Table 1. Material chemical components of the prepared PU composite samples

Sample	PU1	PUC2	PUC3	PUC4	PUC5	PUC6	PUO2	PUO3	PUO4	PUO5	PUO6
MWCNTs(wt %)	0	0.125%	0.25%	0.5%	1%	2%	0	0	0	0	0
OH-MWCNTs(wt %)	0	0	0	0	0	0	0.125%	0.25%	0.5%	1%	2%

Just Accepted

2.3 Tribological testing and characterization

Tribological tests were performed using a rotary friction and wear testing machine (UMT-5, Bruker, USA) in a pin-on-disk configuration, as illustrated in Figure 2. A ZCuSn10Zn2 tin-bronze pin was used as the upper specimen, while the polyurethane composite disks were used as the lower specimens. Tin bronze was selected because it is widely used in marine stern-shaft bearings, allowing the test to better simulate practical water-lubricated operating conditions. The tin-bronze pin had a diameter of 4 mm, and the polyurethane disk specimens had a diameter of 24 mm and a thickness of 8 mm. All tests were

conducted under water-lubricated conditions. During testing, the pin remained stationary, while the polyurethane disk was rotated by a stepper motor. The normal load was applied vertically, and the temperature was maintained at 25 ± 2 ℃. Each test lasted for 1 h. Prior to testing, all specimen surfaces were sequentially polished using 600, 1200, 2400, and 4000 grit sandpapers to ensure comparable initial surface roughness. Each test condition was repeated three times to ensure reproducibility and reliability.

To monitor the friction-induced vibration response, a laser Doppler vibrometer was used to record vibration signals during the friction process. Vibration signals were acquired at two representative stages: the running-in stage and the steady-state friction stage. Specifically, continuous vibration signals were recorded for 0.5 s at 60 s after the start of the test and for 0.5 s at 1600 s, respectively. The recorded vibration velocity signals were processed using the root mean square (RMS) method to quantitatively evaluate the vibration intensity and the vibration attenuation capability of the polyurethane composites. The RMS value was calculated as follows:

$$RMS = \sqrt{\frac{1}{N}\sum_{i=1}^{N} a_i^2} \qquad (1)$$

where x_i is the vibration velocity amplitude measured by the laser Doppler vibrometer at the i-th sampling point, and N is the total number of sampling points. The laser Doppler vibrometer directly outputs vibration velocity signals; therefore, x_i represents the velocity amplitude. When acceleration signals are required for further analysis, they can be obtained by differentiating the velocity signals with respect to time.

$$\eta_v = \left(1 - \frac{RMS_{composite}}{RMS_{matrix}}\right) \times 100\% \qquad (2)$$

where η_v is the vibration attenuation efficiency, and $RMS_{composite}$ and RMS_{matrix} are the RMS values of the polyurethane composite and the neat polyurethane matrix under the same testing condition, respectively. A higher η_v value indicates a stronger vibration attenuation capability of the composite.

After tribological testing, the wear-surface morphology and material characteristics were further analyzed. The mechanical properties of the materials were evaluated using a universal testing machine (TH5000-20C, Tianhui Experimental Machinery, China), with each specimen tested three times and the results averaged. Wear-surface topography was measured using a three-dimensional white-light interferometer (NewView 8300, Zygo, USA), while the microscopic morphology and elemental distribution of the worn surfaces were examined using a field-emission scanning electron microscope

Just Accepted

(SEM, SU8220, Hitachi, Japan). The molecular structure of the polyurethane nanocomposites was analyzed using a Fourier-transform infrared spectrometer (FTIR, Hyperion II, Bruker, Germany) within a scanning range of 4000–400 cm^{-1}, and the surface chemical composition was determined using an X-ray photoelectron spectrometer (XPS, PHI Quantera II, Ulvac-Phi, Japan).

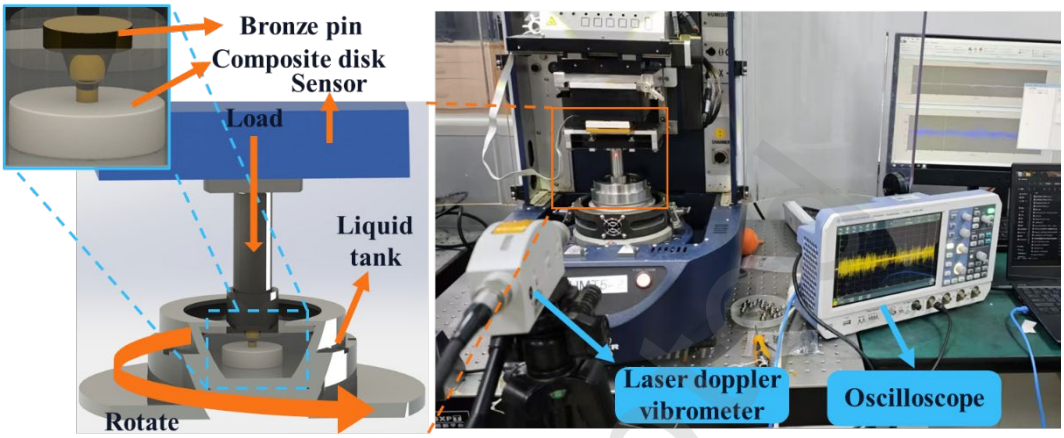


Figure 2. Schematic diagram of friction vibration test

3. Results

3.1 Chemical components analysis

Just Accepted

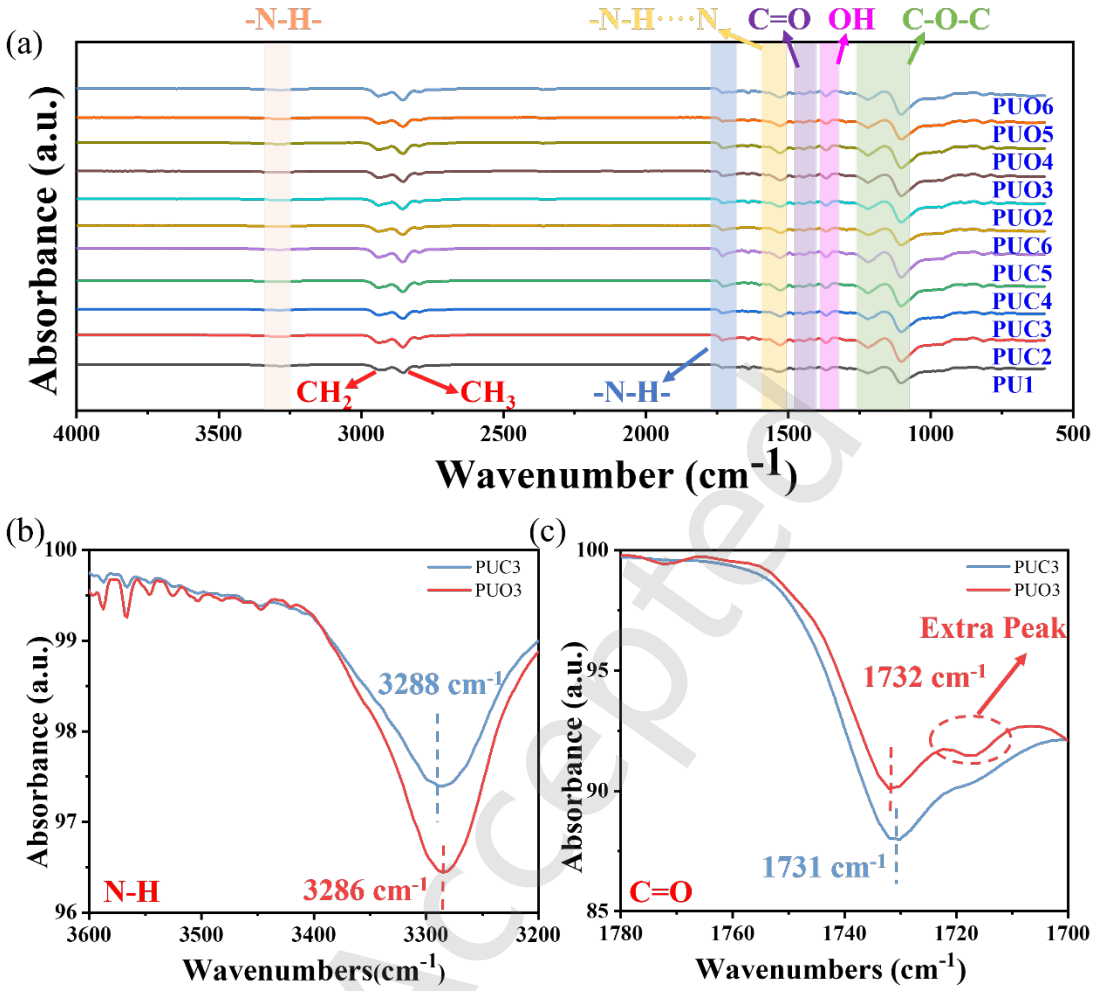


Figure 3. (a) FTIR spectral curves of polyurethane composite materials (b) Infrared spectrum of N-H bonds (c) Infrared spectrum of C=O bonds

FTIR spectra of all samples are presented in Figure 3(a). All composites exhibit the characteristic absorption bands of polyurethane, including the N–H stretching vibration at 3300–3500 cm $^{-1}$, the urethane C=O stretching vibration at 1700–1750 cm $^{-1}$, and the urethane N–H bending vibration (urethane II band) at 1530–1510 cm $^{-1}$, confirming the successful formation of the PU structure. Although the overall spectral profiles do not show significant macroscopic differences due to the relatively low filler content, clear variations appear in the magnified regions. As shown in Figures 3(b) and 3(c), the chemically grafted samples display a distinct red shift and broadening of the C=O stretching vibration peak, together with a shift of the N–H stretching vibration from ~3330 cm^{-1} toward lower wavenumbers and pronounced changes in peak intensity and shape. In contrast, the peak positions of physically blended samples remain essentially unchanged, exhibiting only minor variations in intensity. These spectral changes indicate that fundamental structural alterations occur during the chemical grafting process. The

Just Accepted

hydroxyl groups on the OH-MWCNT surfaces react with isocyanate groups to form new urethane bonding structures, which leads to reconstruction of the hydrogen-bonding network between polyurethane molecular chains[42, 54]. The formation of chemical bonds not only establishes covalent connections between nanoparticles and the polymer matrix but also generates additional hydrogen bonds and intermolecular forces within the system[55, 56]. This chemical modification has profound effects on the material's microstructure. Hydrogen-bond-induced group aggregation promotes microphase separation, forming rigid microdomains centered on hard segments and flexible microdomains centered on soft segments, thereby enhancing the degree of microphase separation[57]. It is noteworthy that although the incorporation of OH-MWCNTs forms a stable network structure, it does not alter the basic main-chain backbone of PU. The changes in peak intensity mainly reflect optimization and adjustment of the microphase separation structure within PU.

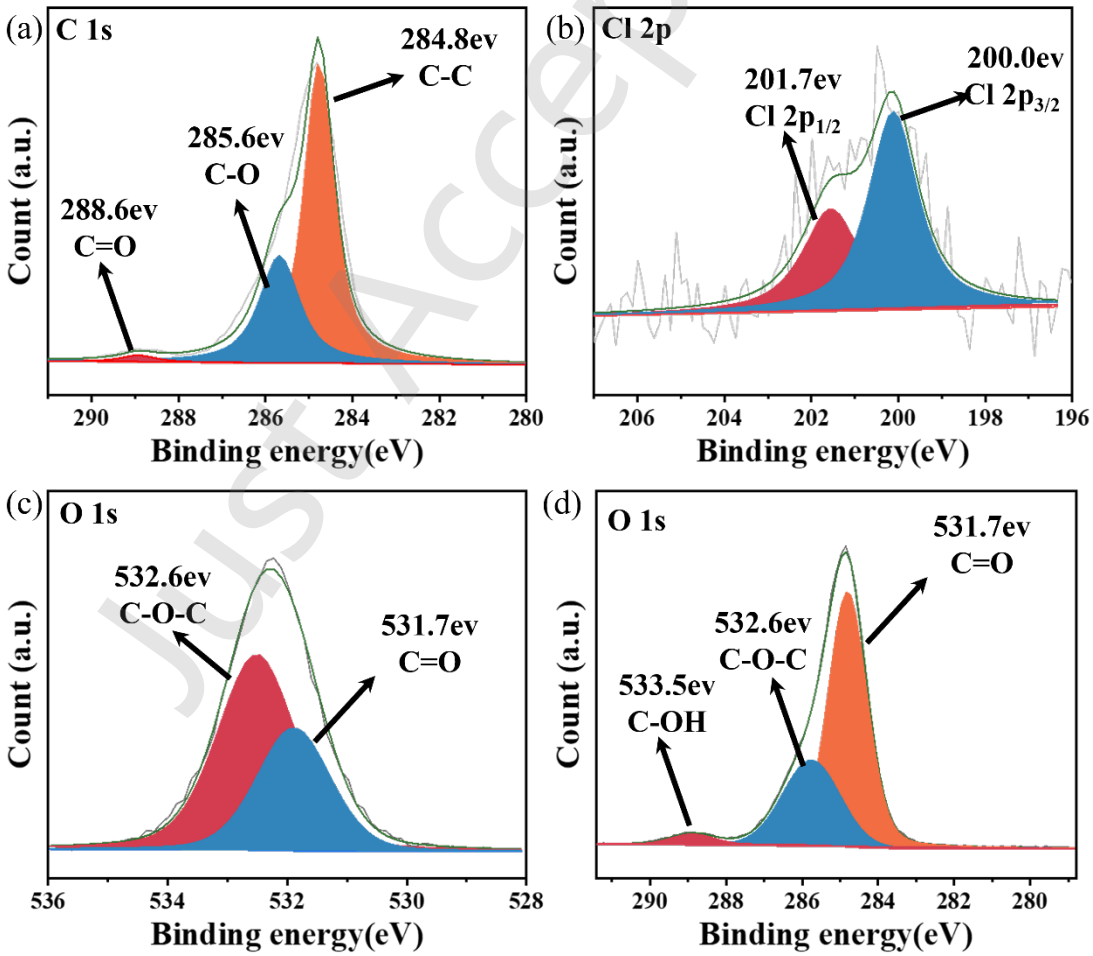


Figure 4. XPS analysis of polyurethane composite materials (a) C (b) Cl (c) O of physical blending samples (d) O of chemical grafting samples

To elucidate the interfacial bonding differences between physical blending and chemical grafting

Just Accepted

samples, high-resolution XPS testing is performed on the PU composites. The results are shown in Figure 4. All spectra are charge-corrected using C 1s = 284.8 eV as an internal standard, a method that is widely proven suitable for polymer and composite systems [58]. The C 1s spectrum shows three typical components located at 284.8 eV (C–C/C–H), 285.6 eV (C–O), and 288.6 eV (C=O/urethane). Cl 2p appears as doublets at 200 eV and 201.7 eV, corresponding to Cl 2p3/2 and Cl 2p1/2, and these peak positions are consistent with common assignments in polyurethane systems. In contrast, the O 1s spectra exhibit distinct differences: the physical blending sample consists mainly of two peaks at 531.7 eV (C=O carbonyl oxygen) and 532.6 eV (C–O–C ether bond/alcoholic oxygen), while the chemical grafting sample shows an additional high binding energy component at approximately 533.5 eV. This peak can is attributed to the urethane-type C–O environment generated by the reaction between TDI and hydroxyl groups on the OH-MWCNTs surface, with binding energy characteristics consistent with similar high-energy O 1s components in esters or polyurethanes [59]. Combined with the FTIR results of this study, namely the red shift of the C=O peak and changes in N–H stretching vibration peak shape, the XPS results confirm that the chemical grafting process not only introduces new covalent bonds between nano-fillers and polymer segments but also significantly alters the oxygen chemical environment at the interface, thereby forming a fundamental distinction from physically blended samples.

3.2 Mechanical properties of PU composite

Figure 5 compares the tensile mechanical properties of pure polyurethane matrix (PU1), physical blending system (PUC), and chemical grafting system (PUO), aiming to reveal the influence patterns of different modification strategies on the mechanical behavior of materials. From the stress-strain curves (Figure 5a), it can be observed that both modification approaches significantly improve the mechanical properties of polyurethane materials, but exhibit distinctly different characteristics. Notably, all samples show pronounced "concave-down" behavior in the initial tensile stage, which is closely related to the soft-hard segment phase separation structure of polyurethane and its reorganization during deformation, reflects the hysteresis, time-dependent, and stress-softening characteristics in the stress-strain behavior of PU, consistent with the Mullins effect reported in the literature[60].

Figures 5 b, c, and d present quantitative comparisons of elongation at break, tensile strength, and elastic modulus for different samples, respectively. The quantitative results demonstrate that PU1 exhibits typical elastomeric characteristics with relatively low tensile strength (approximately 6–8 MPa),high elongation at break (approximately 400%), and a relatively small elastic modulus. In the PUC

Just Accepted

system, the introduction of carbon nanotubes significantly enhances the elongation at break to approximately 600–700%, with some improvement in tensile strength, while the elastic modulus decreases compared to PU1. This trend indicates that under physical blending conditions, the nanofiller primarily exists in a physically dispersed state with limited interfacial interactions and load transfer efficiency. Slight plasticization or microphase separation may enhance chain-segment mobility, thereby weakening the effective load-bearing capacity of the hard-segment phase and resulting in modulus reduction. Meanwhile, the microscale dispersion of fillers can provide local energy dissipation and microcrack blunting effects, thus manifesting as a slight increase in strength and a significant improved in ductility. Within the PUC series, the tensile properties show a non-monotonic dependence on CNT content. The elongation at break first increases and then decreases with increasing MWCNT content, whereas the elastic modulus reaches a minimum at PUC3 and then recovers at higher CNT contents. The low modulus of PUC3 may be attributed to the disturbance of hard-segment packing and physical crosslinking by physically dispersed MWCNTs, which increases the free volume and chain mobility before an effective rigid load-bearing network is formed. The relatively low elongation of PUC4 may be associated with enhanced restriction on chain extensibility and possible local stress concentration at this CNT content. At higher CNT contents, partial agglomeration may further cause fluctuations in the mechanical properties.

In contrast, the PUO system exhibits the most significant improvement in tensile strength, reaching 12–16 MPa, with elastic modulus also markedly increasing compared with PUC, while the elongation at break is lower than that of PUC. This indicates that the introduction of nanoparticles alters the degree of microphase separation within PU, and the modulus enhancement is more pronounced in the chemical grafting system, reflecting that the hard segment-rich phase provides more "physical crosslinking points" that effectively restricted soft segment chain movement[33]. This result corroborates the enhanced hydrogen bonding network observed in the chemical grafting system through infrared spectroscopy, demonstrating that chemical grafting improves filler dispersion and interfacial bonding by introducing covalent bonds between fillers and polyurethane molecular chains, significantly enhancing stress transfer efficiency and chain constraint capability, and ultimately achieving simultaneous strengthening of both strength and modulus. However, the restricted chain segment freedom results in lower ductility compared to the physical blending system. For the PUO series, the higher tensile strength and elastic modulus are attributed to the stronger covalent bonding and hydrogen-bonding interactions between OH-MWCNTs

Just Accepted

and PU chains, which enhance interfacial stress transfer and restrict segmental motion more effectively than in the physically blended system. At excessive OH-MWCNT contents, filler agglomeration, interfacial saturation, and local stress concentration may reduce the reinforcing efficiency and lead to a decline in the mechanical properties.

In summary, the physical blending system (PUC) primarily enhances overall toughness by improving plastic deformation capability and ductility, but is accompanied by modulus reduction and decreased stiffness. The higher deformability of the PUC samples also makes them more prone to tensile deformation and material transfer during sliding, which facilitates the formation of a relatively stable transfer film on the counterface. The chemical grafting system (PUO) achieves dual enhancement of strength and modulus through strengthened interfacial interactions, but at the expense of some ductility. In contrast, the PUO samples are less likely to undergo obvious plastic deformation and material transfer because of their stronger interfacial bonding, higher strength, and higher modulus; therefore, they are less likely to form an evident transfer film, and their wear resistance mainly arises from the improved load-bearing capacity and resistance to shear damage. These two modification strategies demonstrate differentiated and complementary effects in mechanical property tuning, making them suitable for applications prioritizing flexibility and load-bearing capacity, respectively. Therefore, the tribological behavior is governed not only by strength, modulus, and ductility, but also by the ability of the material to deform and form an effective transfer film during sliding.

Just Accepted

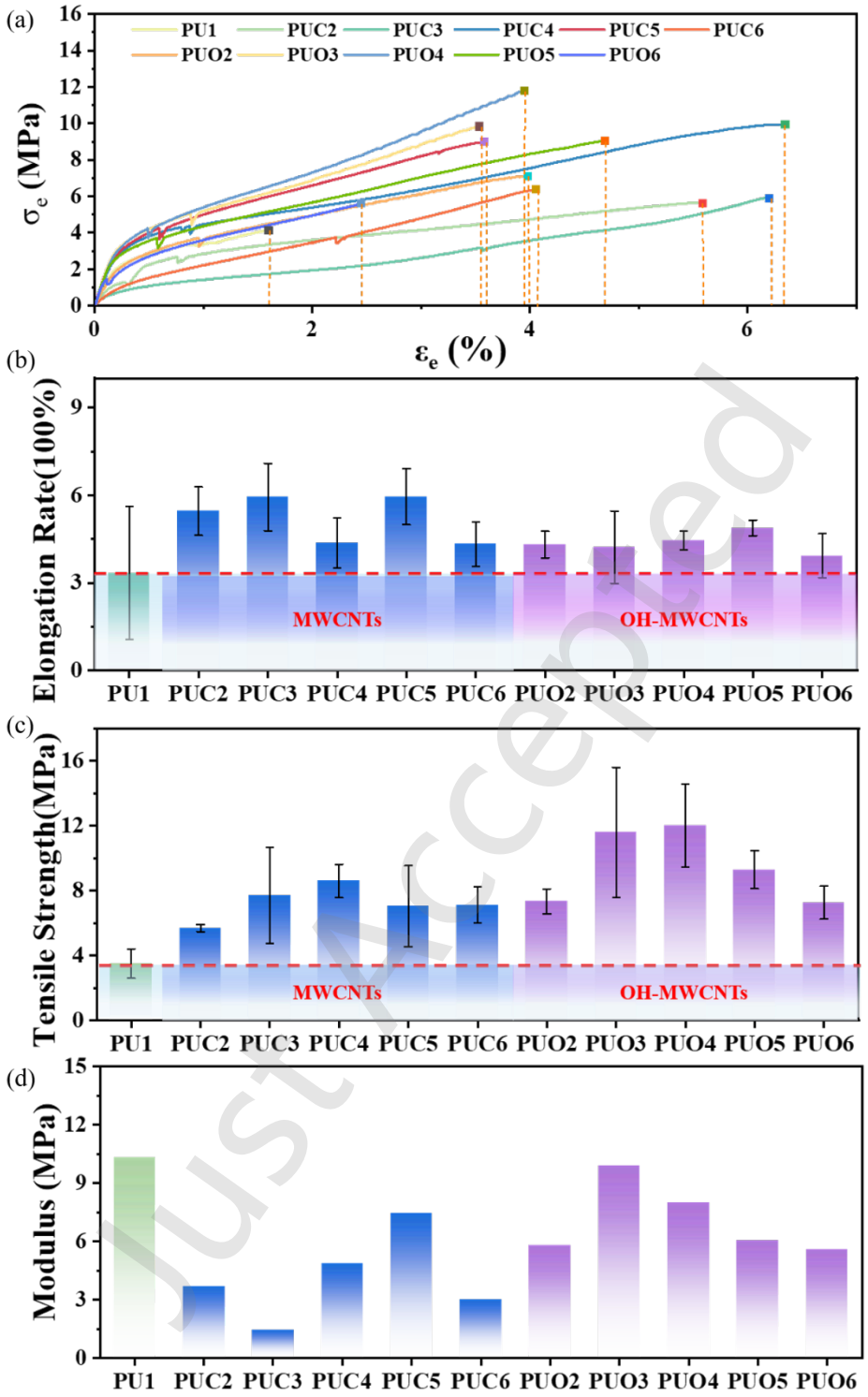


Figure 5. Tensile test results (a) Stress-strain curves (b) Elongation (c) Tensile strength (d) Elastic modulus

3.3 Tribological properties of PU composite

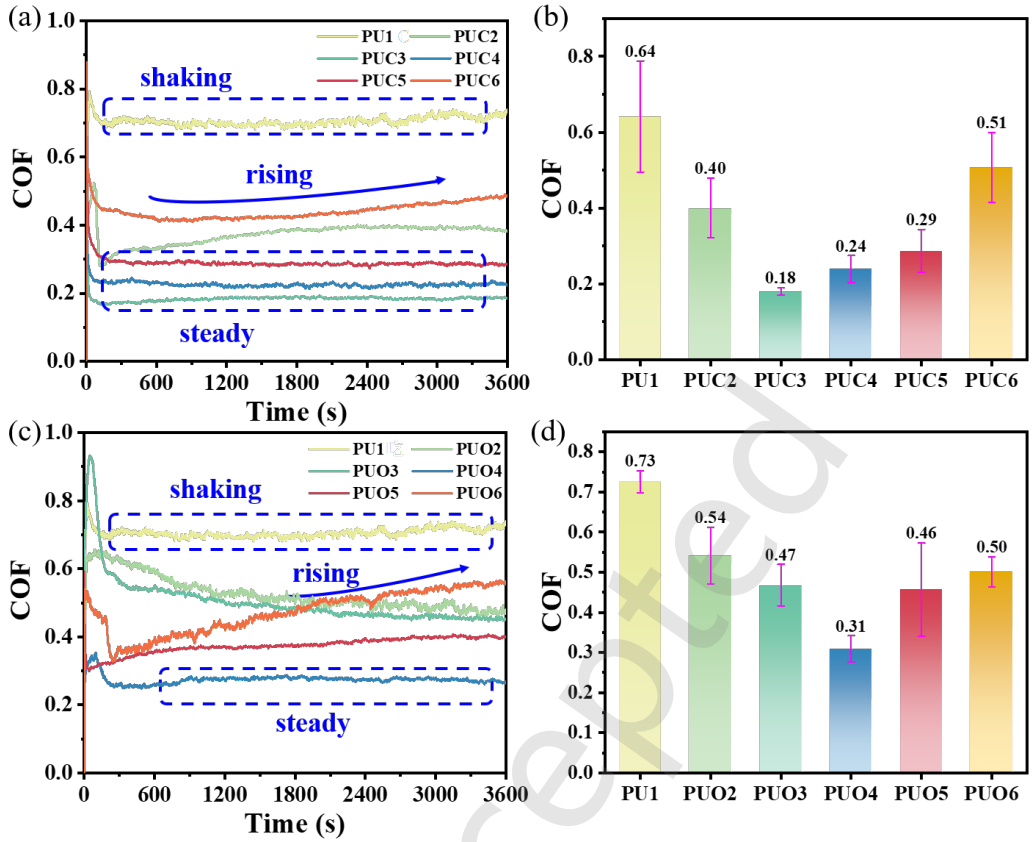


Figure 6. Friction experimental data of polyurethane composite samples (a) COF curves of physical blending group (b) Average COF of physical blending group (c) COF curves of chemical grafting group (d) Average COF of chemical grafting group

The coefficient of friction (COF) is a critical parameter for evaluating the performance of water-lubricated bearings. Figure 6 presents the COF evolution of the composite materials under low-speed, heavy-load water-lubricated conditions. After the running-in stage, neat PU maintains a high COF of approximately 0.7 and exhibits pronounced fluctuations throughout the test, indicating its inadequate tribological performance for long-term service. Both physical blending and chemical grafting markedly reduce the COF and display a similar valley-shaped dependence on nanoparticle content, in which the COF initially decreases and subsequently increases with increasing nanofiller loading. This behavior suggests the presence of an optimal nanoparticle concentration. For physical blending, the COF values of PUC2, PUC3, PUC4, PUC5, and PUC6 are 0.40, 0.18, 0.24, 0.29, and 0.51, respectively, with the best performance observed at 0.25 wt% MWCNT loading (PUC3), corresponding to a 71.9% reduction relative to neat PU. For chemical grafting, the COF values of PUO2, PUO3, PUO4, PUO5, and PUO6 are 0.54, 0.47, 0.31, 0.46, and 0.50, respectively, with the optimal performance occurring at 0.5 wt% OH-MWCNT loading (PUO4), yielding a 57.5% reduction compared with neat PU. The temporal evolution

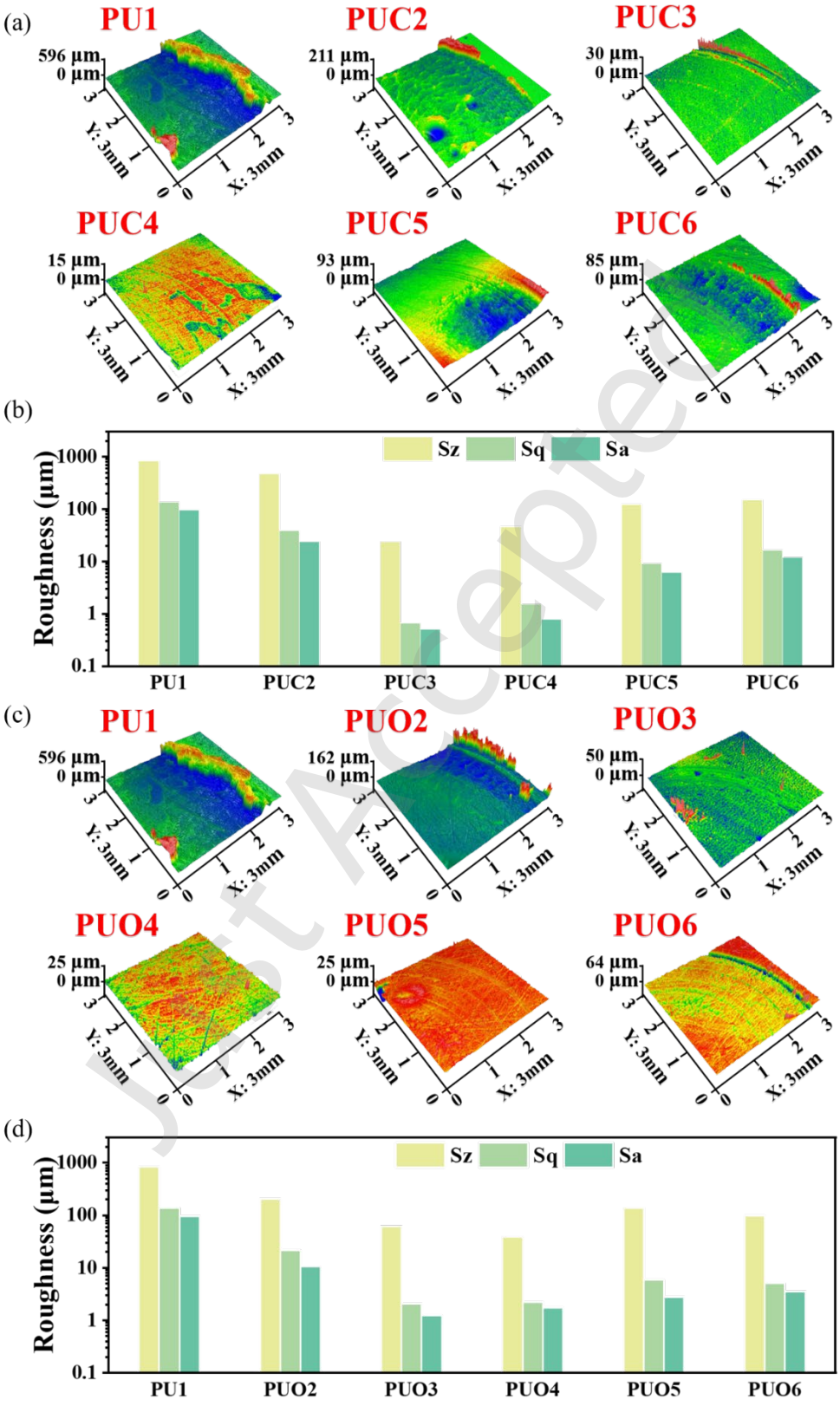
Just Accepted

of COF curves for both modification methods shows comparable trends (Figure 6a and 6c): composites within the optimal loading range maintain stable friction coefficients during the steady-friction stage. In contrast, the CNT/OH-MWCNT content exceeds the optimal range. Excessive filler loading promotes nanotube agglomeration, thereby generating structural defects and local stress-concentration sites in the PU matrix. These defects weaken the mechanical integrity of the composites and reduce their resistance to shear damage during sliding, resulting in an increased friction coefficient. A comparison between Figure 6b and 6d reveals that physical blending provides substantially superior friction-reduction performance compared with chemical grafting. This superiority arises from the distinct reinforcement mechanisms. In physically blended systems, MWCNTs enhance anti-shear behavior primarily through physical interactions that facilitate molecular chain-segment mobility. Conversely, chemical grafting forms covalent bonds between MWCNTs and polymer chains, restricting chain movement and thereby limiting tribological enhancement. This mechanistic explanation is consistent with the higher maximum strain observed in physically blended composites during mechanical testing.

To comprehensively evaluate the tribological performance of the two modification strategies, three-dimensional surface morphology analyses were conducted on the polymer discs after wear testing, with the results presented in Figure 7. A quantitative assessment was carried out using surface roughness parameters, including arithmetic mean height (Sa), root mean square height (Sq), and maximum height (Sz). The results show that both types of modified composites exhibit markedly improved wear resistance compared with pure PU. Notably, the Sa, Sq, and Sz values display a characteristic “valley-shaped” dependence on nanofiller content, consistent with the trends observed in the average friction coefficients. This correlation indicates that samples within the optimal composition range maintain superior surface integrity after tribological testing, exhibiting minimal variations in surface roughness. Comparative analyses of the three-dimensional morphological images further reveal distinct wear mechanisms between the two modification approaches. The physically blended samples (Figure 7a) exhibit more pronounced surface degradation, characterized by higher roughness values and significant plastic deformation, particularly in PUC2, PUC5, and PUC6. These samples show extensive material displacement and surface irregularities, suggesting intensified plastic flow during sliding contact. In contrast, the chemically grafted samples display considerably improved surface stability, featuring relatively smooth worn surfaces and the absence of severe surface damage. This enhanced performance is attributed to the stronger interfacial bonding between the polymer matrix and the grafted MWCNTs,

Just Accepted

which effectively suppresses material removal and plastic deformation under tribological loading.



Just Accepted

Figure 7. Three-dimensional surface morphology of PU composites after wear testing: (a) physically blended modified discs, (b) surface roughness parameters of physical blending group, (c) chemically grafted modified discs, (d) surface roughness parameters of chemical grafting group.

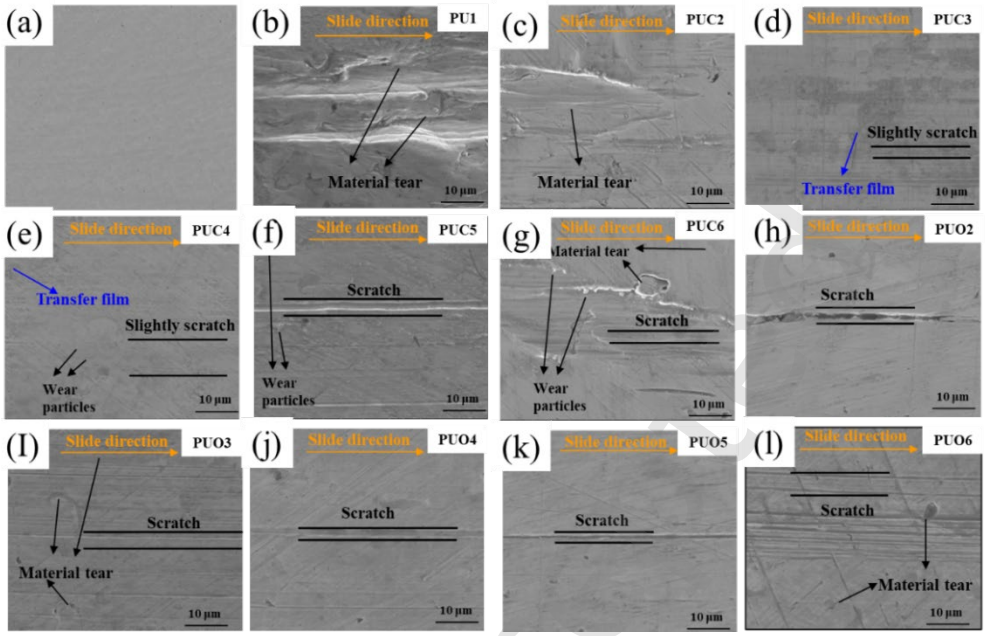


Figure 8. SEM images of upper bronze pin after friction process: (a)Unworn surface, (b)Pure PU, (c, d, e, f, g)Physical blending group, (h, I, j, k, l) chemical grafting group.

Figure 8 presents the SEM analysis of the bronze pin counterpart after tribological testing against the different composite samples. The observed surface morphologies provide important insights into the dominant wear mechanisms governing the sliding interface. For the pure PU group (Figure 8b), the bronze surface exhibits severe adhesive wear, characterized by extensive material tearing and pronounced surface damage. This aggressive wear mode reflects the poor tribological compatibility between pure PU and the bronze counterpart, resulting in substantial material transfer and surface degradation. After modification, both strategies markedly alleviate counterpart wear, although their wear features differ significantly. The physical blending group (Figure 8c–g) predominantly exhibits abrasive wear, as evidenced by the formation of parallel grooves and the presence of wear debris. Although adhesive wear is considerably reduced compared with pure PU, the remaining scratches and localized material transfer indicate persistent mechanical interactions between the sliding surfaces. In contrast, the chemical grafting group (Figure 8h–l) demonstrates superior wear resistance with minimal damage to the bronze surface. Although the chemically grafted group generally shows better wear resistance of the upper bronze pin than the physically blended group, at the optimal nanoparticle mass fraction the

Just Accepted

physically blended composites can induce the formation of a continuous and compact black transfer film on the bronze counterpart (most evident in Figure 8d). This transfer film acts as a stable boundary layer, effectively separating direct metal–polymer contact and accommodating interfacial shear, thereby markedly reducing groove density and abrasive plowing while suppressing localized material transfer and eliminating severe adhesive wear. With the sustained and stable development of this transfer film, the tribological interface evolves toward a more efficient and stable operating regime, enabling the optimally blended system to exhibit overall wear performance superior to that of the chemically grafted group, which suggests the establishment of a more mature, self-adaptive tribological mechanism.

Figure 9 presents the SEM morphological analysis of the modified composite discs after friction testing. The pure PU specimen (Figure 9b) exhibits extensive plastic deformation and a severely irregular worn surface. Under low-speed, heavy-load conditions, the surface undergoes significant degradation and fails to maintain an intact service layer, indicating the material's limited long-term service capability under such operating conditions. Both modification strategies substantially reduce the wear severity of the composites, with wear-state variations that correspond well to the previously observed friction coefficient (COF) trends. The physically blended samples (Figure 9c–g) primarily exhibit plowing grooves characteristic of abrasive wear, along with plastic deformation associated with localized adhesion. Although adhesive wear is markedly reduced compared with pure PU, evident plastic flow features persist, accompanied by a considerable number of wear particles on the worn surface. In contrast, the chemically grafted samples (Figure 9h–l) demonstrate superior wear resistance relative to the physical blending group. This improvement is reflected in two key aspects: (1) a substantial reduction in both wear particle accumulation and adhesion-induced plastic flow morphology, and (2) a dominant transition of the wear mechanism toward plowing-groove features typical of abrasive wear. This shift in wear behavior suggests that chemical grafting effectively enhances the material's anti-wear capability by strengthening interfacial bonding, thereby transforming the wear mode from destructive adhesive wear to relatively mild abrasive wear and significantly improving the overall tribological performance.

Just Accepted

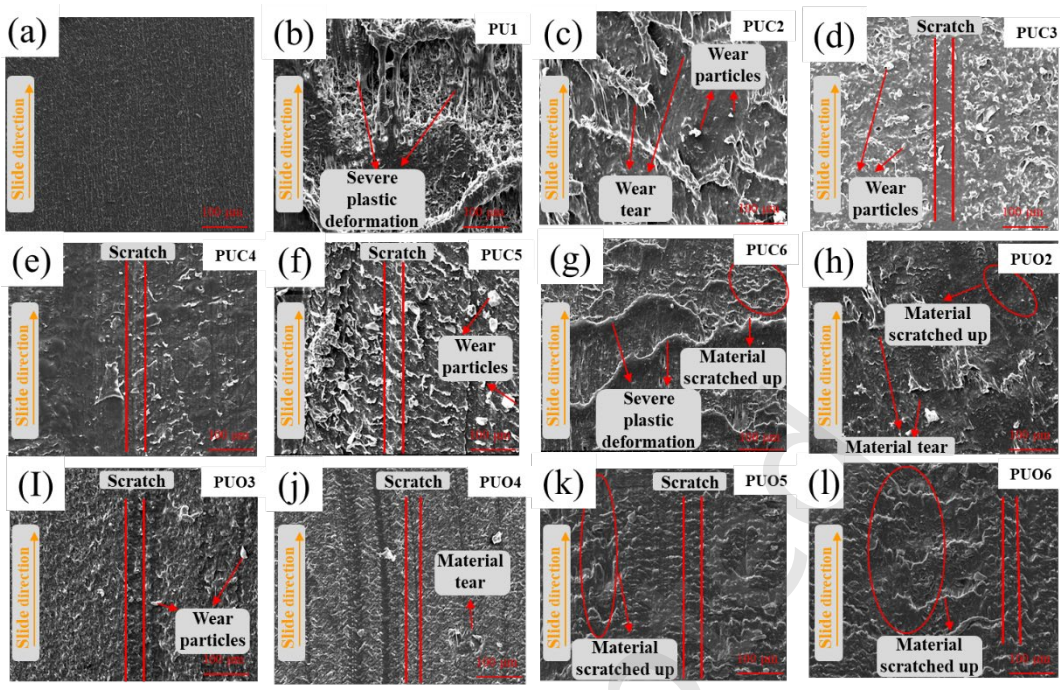


Figure 9. SEM image of modified disc after friction: (a)Unworn surface, (b)Pure PU, (c, d, e, f, g)Physical blending group, (h, I, j, k, l) chemical grafting group.

3.4 Vibration Acceleration Signal Analysis

The vibration characteristics of water-lubricated bearings are critical indicators for assessing their long-term operational stability. Based on the preceding tribological results, the optimal nanoparticle concentration range was determined to be 0.25–0.5 wt%. Therefore, two representative contents, 0.25 wt% and 0.5 wt%, were selected for vibration testing. Vibration signals were collected at 60 s, corresponding to the running-in stage, and at 1600 s, corresponding to the steady-friction stage, to systematically evaluate vibration intensity and stability. To further quantify the vibration response, the RMS values of the vibration signals were calculated, and the vibration attenuation efficiency was determined relative to the pure PU matrix.

The results are shown in Figure 10. Under the 0.25 wt% nanoparticle loading, the physically blended MWCNTs/PU and chemically grafted OH-MWCNTs/PU composites exhibited markedly different vibration-control behaviors. During the running-in stage, the pure PU matrix showed an RMS value of 0.38. In comparison, the physically blended MWCNTs/PU composite exhibited a lower RMS value of 0.21, corresponding to a vibration attenuation efficiency of 73.39%, indicating that the physical blending strategy effectively suppressed friction-induced vibration at the initial stage. By contrast, the chemically grafted OH-MWCNTs/PU composite showed an RMS value of 0.36 and a vibration

Just Accepted

attenuation efficiency of only -0.01%, suggesting that the chemical grafting strategy provided almost no effective damping improvement during the running-in process. Upon entering the steady-state friction stage, the vibration amplitudes of all sample groups decreased significantly. The physically blended MWCNTs/PU composite maintained a low RMS value of 0.21, corresponding to a vibration attenuation efficiency of 45.12%, confirming its stable and effective vibration-suppression capability under steady friction. In contrast, the chemically grafted OH-MWCNTs/PU composite showed a higher RMS value of 0.36 and a much lower attenuation efficiency of 4.84%, indicating limited damping performance. When the nanoparticle content increased to 0.5 wt%, the difference between the two modification strategies became more pronounced: the physical blending group showed further enhancement in vibration suppression, whereas the chemically grafted counterpart exhibited increased overall vibration intensity.

Overall, the RMS-based analysis demonstrates that the physical blending strategy using MWCNTs is more effective in reducing vibration intensity and peak amplitudes, thereby providing superior vibration damping performance compared with chemically grafted OH-MWCNTs/PU composites.

Just Accepted

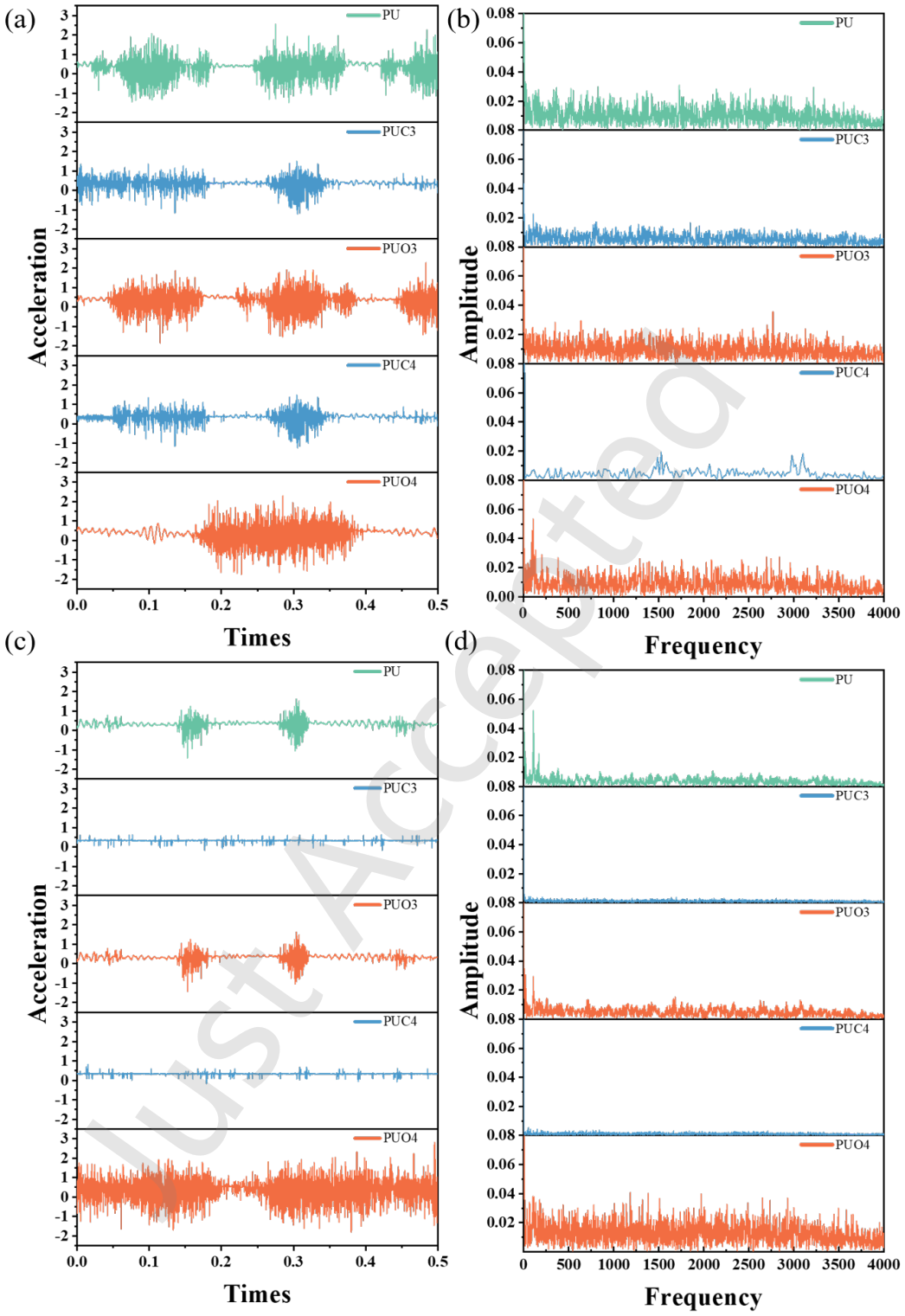


Figure 10. Friction vibration results of samples with mass fractions of 0.25wt% and 0.5wt% (a) Time domain diagram of running-in stage (b) Frequency spectrum diagram of running-in stage (c) Time domain diagram of stable stage (d) Frequency spectrum diagram of stable stage

4. Discussion

The above results clearly show that both COF and wear performance exhibit optimal content ranges,

Just Accepted

with performance deterioration occurring when the nanoparticle concentration deviates from these ranges. Although this behavior is attributed to insufficient nanoparticle loading at low concentrations and aggregation at high concentrations, direct evidence supporting this inference has remained limited. Additionally, the wear tests indicate that chemically grafted samples exhibit superior wear resistance. However, within the optimal concentration range, the physically blended samples display better surface integrity and markedly enhanced vibration damping performance. To further elucidate this seemingly contradictory phenomenon, we conducted a detailed examination of the transfer films formed during tribological testing. Pronounced transfer film formation was observed on the bronze pin surfaces for the physically blended specimens, and the evolution of these films provides compelling evidence for understanding the performance differences between the two modification strategies.

Figure 11 illustrates the morphology evolution of the transfer films on the bronze pin surface in the physical blending group as the nanoparticle mass fraction increases. SEM observations, combined with elemental mapping, confirm evident carbon transfer from the composite disc to the copper surface. The transfer film morphology exhibits three characteristic stages with increasing nanoparticle content. At low mass fractions, the films are discontinuous and sparsely distributed, unable to form an effective protective layer. This directly verifies that insufficient nanoparticle content limits the ability of the physical blending approach to promote ideal transfer film formation. Within the optimal mass fraction range, the transfer films develop into continuous and smooth layers, effectively separating the mating surfaces, preventing direct asperity–asperity contact, suppressing wear, and reducing vibration through mitigation of friction-induced stick–slip behavior. This results in outstanding wear resistance and vibration damping performance. At high mass fractions, however, the transfer films exhibit coarse particle-like structures and localized defects, leading to the onset of three-body abrasive wear. The emergence of these large particulate features strongly supports the conclusion that nanoparticle agglomeration in the composite disc leads to defects, which in turn cause non-ideal, discontinuous transfer film morphology.

Based on the transfer-film analysis, the distinct friction mechanisms of the physically blended and chemically grafted composites under water lubrication can be clearly elucidated. For the physically blended system (Fig. 12a), the nanoparticles are incorporated into the PU matrix through noncovalent interactions. Under applied normal and shear loads, the polymer chains undergo relative motion, and the presence of nanoparticles increases local chain mobility, thereby promoting the generation of transfer materials and facilitating transfer-film formation at the sliding interface. This mechanism contributes to

Just Accepted

the reduction of the friction coefficient; however, the wear resistance is governed by nanoparticle dispersion and interfacial stability, making the tribological performance highly sensitive to nanoparticle concentration. In contrast, for the chemically grafted system (Fig. 12b), the nanoparticles are covalently anchored to the PU backbone, substantially enhancing interfacial adhesion. Under shear loading, the material exhibits a more robust internal structure, and reconstruction of the hydrogen-bond network further improves shear resistance and wear performance. Nevertheless, the restricted chain mobility suppresses the development of a sufficient transfer film, rendering the system more susceptible to stick–slip behavior and, in certain cases, resulting in vibration-damping performance inferior to that of neat PU. Further analysis of the evolving interfacial behavior at different nanoparticle concentrations (Fig. 12c) reveals an even sharper contrast between the two modification strategies. In the physically blended composites, low nanoparticle concentrations enhance chain relaxation and mobility but do not provide enough transfer material to form a continuous protective film, leading to pronounced plastic deformation. As the nanoparticle concentration increases, chain mobility is further intensified; however, agglomeration-induced interfacial defects promote the formation of wear debris and accelerate wear. In comparison, the chemically grafted composites maintain strong interfacial bonding and consistently high wear resistance across the entire concentration range, but the suppressed chain dynamics hinder the formation of smooth, continuous transfer films.

Overall, the fundamentally different tribological behaviors of the two systems arise from the distinct ways in which nanoparticles regulate chain mobility, which ultimately determines transfer-film quality and governs the stability of the sliding interface.

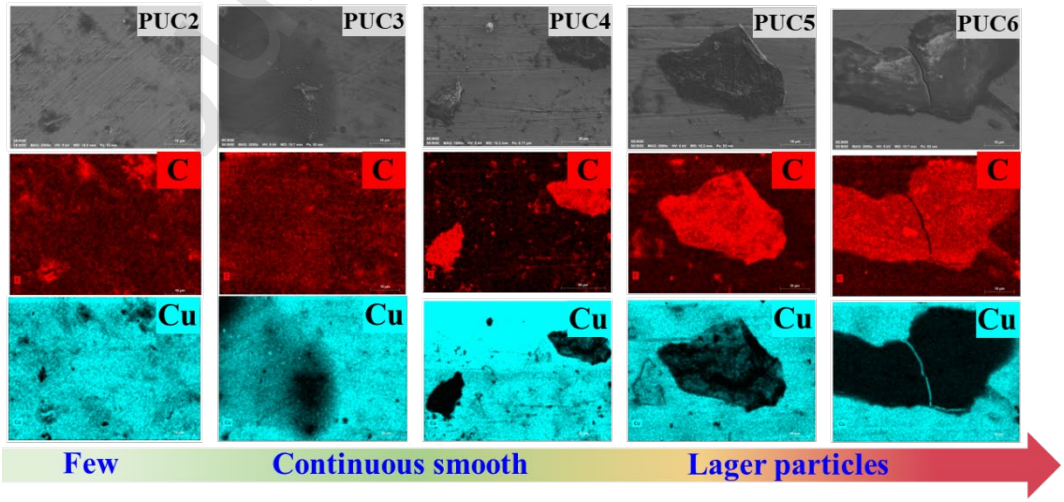


Figure 11. SEM morphologies and EDS elemental distribution of C and Cu in transfer films for samples

Just Accepted

PUC2-PUC6.

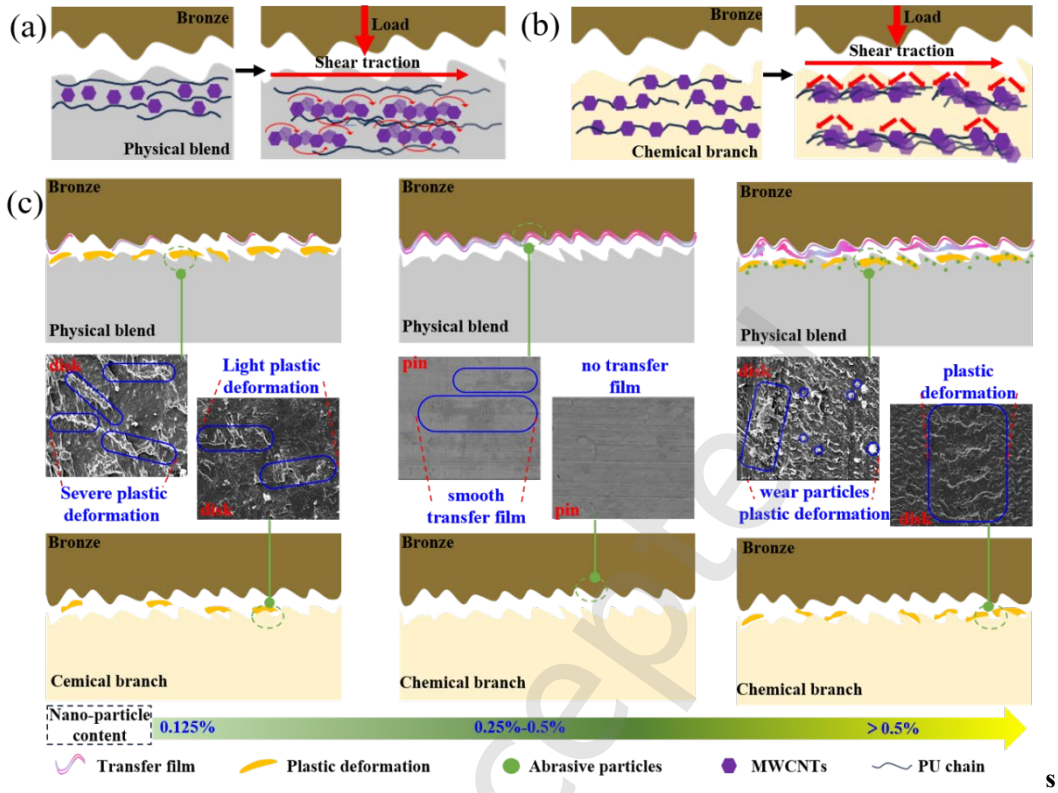


Figure 12. Schematic illustration of the friction mechanisms of PU nanocomposites. (a) Physical blending: nanoparticles roll easily and chains slide readily under load. (b) Chemical grafting: strong interfacial bonding restricts chain mobility. (c) Evolution of interfacial contact and transfer-film morphology with increasing nanoparticle content.

5. Conclusions

This study was driven by the performance requirements of water-lubricated bearings used in marine propulsion systems, where low friction, vibration suppression, and long-term wear stability are essential under corrosive and particle-contaminated environments. Polyurethane (PU) nanocomposites modified via physical blending (MWCNTs) and chemical grafting (OH-MWCNTs) were systematically investigated using in-situ polymerization. FTIR and XPS analyses confirmed that chemical grafting introduces new urethane linkages through reactions between hydroxyl functionalities and isocyanate groups, accompanied by reconstruction of the hydrogen-bond network, whereas physical blending preserves the original molecular structure. The two modification routes produced fundamentally different material responses. Physically blended composites exhibited enhanced ductility, substantial friction reduction (up to 71.9%), and excellent vibration-damping capability. In contrast, chemically grafted

Just Accepted

composites demonstrated significantly increased tensile strength (12–16 MPa), higher stiffness, and superior wear resistance, attributed to a transition from adhesive to abrasive wear mechanisms. Transfer-film analyses further elucidated the origins of these differences: physical blending increased chain mobility, enabling the formation of continuous and smooth transfer films at optimal filler levels (0.25–0.5 wt%), which effectively suppressed stick–slip behavior and ensured stable low-friction operation. Conversely, covalent bonding in chemically grafted PU restricted segmental motion, enhancing structural robustness but limiting energy-dissipation capability.

Overall, these findings clarify the structure–property relationships governing PU-based nanocomposites and highlight the complementary advantages of the two modification strategies. Physical blending is better suited for water-lubricated bearing applications where friction reduction and vibration suppression are prioritized, whereas chemical grafting is more appropriate for load-bearing components requiring high strength and wear resistance. These insights provide practical guidance for selecting tailored modification approaches for advanced tribological applications.

6.Acknowledgements

The authors acknowledge financial support from the National Science Fund for Distinguished Young Scholars (No. 52501412), the National Science Fund for Distinguished Young Scholars (No. 52405172) and the Fundamental Research Funds for the Central Universities (2024ZKPYJD09).

Just Accepted

7. References

[1] ZHU C, CHEN Q, LIU X. Review of advanced fabric composite liners for enhancing tribological performance on self-lubricating joint bearings. *Surface Science and Technology* **3**(1): 4 (2025)

[2] ZHANG X, NING C, OUYANG W, et al. In-situ wear monitoring of water-lubrication thrust bearings based on ultrasonic reflection coefficient amplitude spectrum and transfer function. *Wear* **570**: 205905 (2025)

[3] XU M, WANG Z, GUO L, et al. Tribological properties of PTFE-based fabric composites at cryogenic temperature. *Friction* **12**(2): 245-57 (2024)

[4] CHEN Z, WANG C, LIU Y, et al. The effect of lateral size of few-layer graphene oxide sheets as aqueous lubricant additives. *Friction* **13**(8): 9441030 (2025)

[5] GUO W, ZHAO L, QIN Z, et al. Bioinspired self-adhesive coating for surface functionalization of medical devices with lubrication and antibacterial properties. *Friction* **13**(11): 9440926 (2025)

[6] ZHANG X, CHEN Q, CHEN K, et al. Robust hydrogels with orderly assembly of hydroxyapatite induced by temperature gradient. *Friction* **13**(11): 9441046 (2025)

[7] XIONG D, GONG C, SHI Z, et al. Boundary film–liquid mixed lubrication of biomimetic lubricants on cartilage interfaces. *Friction* **13**(9): 9441029 (2025)

[8] XU S, ZHANG Y, ZHOU J, et al. 20 - Tribology of polymer gears: friction coefficient and wear. In: *Polymer Gears*. THOMAS S, HUSKIĆ M, MARIA H J, et al., Ed.: Elsevier, 2025: 495-514.

[9] KALáCSKA Á, COEN A, POLETTO J C, et al. Tribological Investigation of Polymer Composite Dynamic Shaft Seals in Extraterrestrial Applications. *Journal* https://doi.org/10.3390/lubricants12120451 (2024)

[10] SHAN Z, JIA X, QIU Y, et al. Flexible carbon fiber/epoxy resin-based self-lubricating composites reinforced by continuously regenerated lignocellulose and MoS2 nanosheets. *Friction* **13**(10): 9441054 (2025)

[11] XU J, HAN T, ZHANG C, et al. Differential hydration lubrication performance of polyelectrolyte-modified UHMWPE promoted by diverse charge characteristics. *Friction* **13**(8): 9441006 (2025)

[12] GONG H, SONG Y, LI G L, et al. An intelligent polymer composite with self-lubricating and self-healing functionalities. *Composites Part B: Engineering* **260**: 110776 (2023)

Just Accepted

[13] WANG R, ZHANG F, YANG K, et al. Review of two-dimensional nanomaterials in tribology: Recent developments, challenges and prospects. *Advances in Colloid and Interface Science* **321**: 103004 (2023)

[14] XU Q, TANG X, ZHANG J, et al. Unraveling Tribochemistry and Self-Lubrication Mechanism of Polytetrafluoroethylene by Reactive Coarse-Grained Molecular Dynamics Simulations. *ACS Applied Materials & Interfaces* **15**(38): 45506-15 (2023)

[15] FENG X, ZHU P, WANG W. Lubricant seepage behavior of porous polyimide cage materials under sliding contact loading. *Tribology International* **204**: 110470 (2025)

[16] SHU H, CUI J, LIU Y, et al. MAP-inspired dual crosslinked PVP-phenol sprayable hydrogel coating for stable marine antifouling applications. *Friction* **13**(11): 9440946 (2025)

[17] ZHANG K, CHEN Q, ZHANG Y, et al. Numerical and experimental investigations on thermoelastic hydrodynamic performance of planetary gear sliding bearings in wind turbine gearboxes. *Tribology International* **191**: 109081 (2024)

[18] LIU Y, ZHOU Y, WANG W, et al. Synergistic damage mechanisms of high-temperature metal corrosion in marine environments: A review. *Progress in Organic Coatings* **197**: 108765 (2024)

[19] PEI W, PEI X, XIE Z, et al. Research progress of marine anti-corrosion and wear-resistant coating. *Tribology International* **198**: 109864 (2024)

[20] REJITH R, KESAVAN D, CHAKRAVARTHY P, et al. Bearings for aerospace applications. *Tribology International* **181**: 108312 (2023)

[21] MUKHTAR S H, GULZAR A, SALEEM S, et al. Advances in development of solid lubricating MoS2 coatings for space applications: A review of modeling and experimental approaches. *Tribology International* **192**: 109194 (2024)

[22] LUO H, LIU S, LI Z, et al. Onion-shell nuclei on monolayer MoS2 facilitate friction reduction. *Friction* **13**(7): 9440981 (2025)

[23] WEI P, HOU X, HAN S, et al. Superlubrication of poly-α-olefin-8 (PAO8) enabled by MXene/PI coating. *Friction* **13**(6): 9440967 (2025)

[24] JIANG S, PUHAN D, HUANG J, et al. Tribological properties of graphene-reinforced polyurethane bearing material. *Tribology International* **193**: 109481 (2024)

[25] PATEL Y, JOSHI U, JAIN P, et al. Tribological performance of graphene oxide reinforced PEEK nanocomposites with machine learning approach. *Results in Engineering* **24**: 103423 (2024)

Just Accepted

[26] XUE L, XU Q, MENG C, et al. Achieving the ultra-low friction and wear rate of PEEK-PTFE composites by Ti3C2Tx MXene reinforcement. *Tribology International* **199**: 110030 (2024)

[27] YAN J, WANG Y, LIU F, et al. Enhancing the tribological performance of polyimide composite coatings with amino-functionalized MXene nanofillers. *Tribology International* **200**: 110064 (2024)

[28] YE Q, CHEN X, ZHANG X, et al. Improvement of tribological and anti-corrosive performance of MXene nanosheets by grafting polymer brush. *Tribology International* **201**: 110198 (2025)

[29] CHEN Z, ZHANG M, REN P, et al. Enhanced mechanical and tribological properties of epoxy composites reinforced by novel hyperbranched polysiloxane functionalized graphene/MXene hybrid. *Chemical Engineering Journal* **466**: 143086 (2023)

[30] HE Y, FAN X, HUANG Y, et al. Experimental and theoretical evaluations on the parallel-aligned graphene oxide hybrid epoxy composite coating toward wear resistance. *Carbon* **217**: 118629 (2024)

[31] LIU Y, CAI M, XIE Z, et al. Multiple molecular chains grafted graphene oxide chelated with cerium cation towards anti-corrosion and anti-wear application. *Applied Surface Science* **703**: 163444 (2025)

[32] WANG Q, ZHANG N, ZHANG X, et al. Dynamic covalent chemistries of thermosetting polymer for recyclability and intelligent lubrication. *Friction* **13**(4): 9440925 (2025)

[33] HUANG M, LI Z, XU W, et al. Visualization and quantification of microphase separation in thermoplastic polyurethanes under different hard segment contents and its effect on the mechanical properties. *Polymer Testing* **131**: 108329 (2024)

[34] SHAN J-W, ZHU Y-B, NI L-L, et al. Viscoelastic Property Evolution of Thermoplastic Polyurethane during Annealing Treatment and Its Correlation with Segmental Crystallization. *Chinese Journal of Polymer Science* **42**(12): 1976-85 (2024)

[35] KIM D, KIM G, JANG J, et al. Analysis of low-frequency fatigue behavior of polyurethane elastomers under localized compressive loading using shear creep behavior. *Polymer Testing* **149**: 108864 (2025)

[36] HAN X, WANG D, CHEN X, et al. High damping polyurethane elastomers with wide temperature ranges. *Polymer* **325**: 128307 (2025)

[37] HE Y, ZHANG Y, XU X, et al. Enhancement on the thermal and tribological behaviors of

Just Accepted

polyurethane/epoxy-based interpenetrating network composites by orientationally aligned CNF/MXene/WPU aerogels. *Composites Part A: Applied Science and Manufacturing* **187**: 108477 (2024)

[38] ZHANG L, DONG C, YUAN C, et al. Production and tribological behaviours of self-lubricating polyurethane-based damping composites with enhanced wear resistance and vibration attenuation. *Wear* **571**: 205827 (2025)

[39] LI F, MA Y, CHEN L, et al. In-situ polymerization of polyurethane/aniline oligomer functionalized graphene oxide composite coatings with enhanced mechanical, tribological and corrosion protection properties. *Chemical Engineering Journal* **425**: 130006 (2021)

[40] LIU Y, SHEN Y, LI X, et al. Transparent and mechanically robust Polyvinyl-alcohol nanocomposites based on multiple cross-linked networks for paper-reinforcement Technology. *Chemical Engineering Journal* **446**: 136896 (2022)

[41] SONG Y, LI J, WANG X, et al. Grafting isocyanate onto graphene oxide for polyurethane composites to improve their thermal stability and mechanical properties. *Iranian Polymer Journal* **33**(1): 45-55 (2024)

[42] WANG C, CHEN X, XIE H, et al. Effects of carbon nanotube diameter and functionality on the properties of soy polyol-based polyurethane. *Composites Part A: Applied Science and Manufacturing* **42**(11): 1620-6 (2011)

[43] FENG Z, SHAO M, XU M, et al. Study on the tribological properties of MXene reinforced polyurethane composites under dry conditions. *Tribology International* **202**: 110348 (2025)

[44] TALAPATRA A, DATTA D. Experimental and molecular dynamics simulation based investigation to understand tribological performance of graphene reinforced thermoplastic polyurethane (Gr/TPU) nanocomposites. *Tribology International* **196**: 109703 (2024)

[45] ZAFAR S, KAHRAMAN R, SHAKOOR R A. Silane functionalization of titania-graphene oxide nanocomposite for superior anticorrosion polyurethane coatings on steel. *Colloids and Surfaces A: Physicochemical and Engineering Aspects* **703**: 135434 (2024)

[46] WAN J, YE D. Waterborne polyurethane adhesives grafted with carbon dots for enhancing dispersion, cohesion, and adhesion. *International Journal of Adhesion and Adhesives* **140**: 104031 (2025)

[47] LV J, LI X, ZHAI N, et al. Mechanically responsive self-reinforced polyurethane elastomers

Just Accepted

with cyclodextrin metal-organic framework structure for high impact resistance. *Chemical Engineering Journal* **522**: 166870 (2025)

[48] LIU N, LI S, WANG X. Mechanism of coupling polymer thickness and interfacial interactions on strength and toughness of non-covalent nacre-inspired graphene nanocomposites. *Composites Science and Technology* **241**: 110124 (2023)

[49] SHI J, YIN S, LI H, et al. Operando formation of hydration layer and tribofilm of graphene oxide for achieving synergistic lubrication on electrochemical boronizing surface. *Carbon* **235**: 120089 (2025)

[50] ZHAO S, HUA C, ZHAO Y, et al. Casting of regulable nanostructured transfer film by detaching nanofiller from the composite into the tribosystem – A strategy to customize tribological properties. *Tribology International* **195**: 109597 (2024)

[51] ZAHARIN H A, GHAZALI M J, THACHNATHAREN N, et al. Advancements in MXene-based nanomaterials for tribological applications: Comprehensive review and future prospects. *Tribology International* **208**: 110665 (2025)

[52] TAGHIZADEH TABRIZI A, ENZINGER N. 2D materials enhancing tribological performance in bulk and composite coatings: a review. *Graphene and 2D Materials* **9**(3): 275-88 (2024)

[53] RAMTEKE S M, WALCZAK M, DE STEFANO M, et al. 2D materials for Tribo-corrosion and -oxidation protection: A review. *Advances in Colloid and Interface Science* **331**: 103243 (2024)

[54] YANG X, HONG J, XIONG Z, et al. Performance of PTMEG/CO composite polyurethane and modification mechanism of polyurethane-modified asphalt. *Construction and Building Materials* **475**: 141117 (2025)

[55] WEI K, CAO X, TANG B, et al. Castor oil-based polyurethane Vitrimer modified asphalts regulated by dual dynamic reversible reactions and crosslinking density: Preparation, basic assessment and self-healing behavior. *Construction and Building Materials* **429**: 136430 (2024)

[56] XIA W, SUN B, HE Y, et al. Effect of disulfide bond content on thermal-healing properties of castor oil-based polyurethanes. *Polymer Degradation and Stability* **229**: 110943 (2024)

[57] CHENG B-X, GAO W-C, REN X-M, et al. A review of microphase separation of polyurethane: Characterization and applications. *Polymer Testing* **107**: 107489 (2022)

[58] GRECZYNSKI G, HULTMAN L. X-ray photoelectron spectroscopy: towards reliable binding energy referencing. *Progress in Materials Science* **107**: 100591 (2020)

Just Accepted

[59] LóPEZ G P, CASTNER D G, RATNER B D. XPS O 1s binding energies for polymers containing hydroxyl, ether, ketone and ester groups. *Surface and interface analysis* **17**(5): 267-72 (1991)

[60] QI H J, BOYCE M C. Stress–strain behavior of thermoplastic polyurethanes. *Mechanics of materials* **37**(8): 817-39 (2005)

Author biography



Jie Cheng is a professor at the School of Mechanical and Electrical Engineering, China University of Mining and Technology-Beijing, China. She obtained her Ph.D. degree from Tsinghua University, China, in 2016 and her B.S. degree from Shandong University, China, in 2011. She worked as a postdoctoral fellow at Tsinghua University, China, and KTH Royal Institute of Technology, Sweden, from 2017 to 2019. She received the Young Elite Scientists Sponsorship Program from the China Association for Science and Technology (CAST) in 2022. Her research interests emphasize the use of corrosion science, tribology technology, and surface and interface techniques in the following areas: (1) chemical mechanical polishing (CMP) technology in integrated circuit fabrication for advanced technology nodes; (2) ultraprecision manufacturing methods for coal electronics materials; and (3) the mechanism of corrosion wear and the development of bioinspired green multifunctional coatings for engineering purposes.



Shimao Han received his B.S. degree from China University of Mining and Technology, Beijing, China, in 2023. Now he is a Ph.D. candidate at China University of Mining and Technology, Beijing, China. His current research focuses on the friction mechanisms of water-lubricated bearings and corrosion–vibration-reduction coupling phenomena.

Just Accepted